Comprehensive Global Energy Minimum Modeling of the Sarin−Serine Adduct

Jing Wang,[†] Szczepan Roszak,[†,‡] Jiande Gu,*[,†,§] and Jerzy Leszczynski*[,†]

Computational Center for Molecular Structure and Interactions, Department of Chemistry, Jackson State University, Jackson, Mississippi 39217, Institute of Physical and Theoretical Chemistry, Wroclaw University of Technology, Wyb. Wyspiansliego 27 50370, Wroclaw, Poland, and Drug Design & Discovery Center, State Key Laboratory of Drug Research, Shanghai Institute of Materia Medica, Shanghai Institutes for Biological Sciences, Chinese Academy of Sciences, Shanghai 200031 P. R. China

Received: August 19, 2004; In Final Form: October 26, 2004

DFT-based molecular dynamics and quantum chemistry theory approaches are combined to investigate the various conformers of sarin−serine adduct. Twenty different conformers have been located as the local minima on the potential energy surface. They are categorized into five classes based on the relative orientation of sarin moiety. The energy properties of the twenty sarin−serine conformers revealed in the present study suggest that at least four of the conformers (**1**−**1**, **4**−**1**, **4**−**2**, and **5**−**1**) are expected to have crucial contributions to the phosphonylation and dealkylation reactions of the sarin−serine adduct at low temperature. Among them, the **1**−**1** conformer which has both the lowest energy and the highest Boltzman distribution relative probability is expected to be the most important. However, as the temperature rises, the **4**−**1** conformer plays a more important role than **1**−**1** in the sarin−serine adductation reactions. Under the relatively high temperatures, the contribution of conformer **5**−**1** decreases in the phosphonylation and dealkylation reactions while at least eight other conformers (**1**−**2**, **1**−**3**, **3**−**1**, **3**−**4**, **3**−**7**, **4**−**2**, **4**−**3**, and **4**−**4**) are expected to have larger contributions in these reactions.

1. Introduction

Acetylcholinesterase (AChE) hydrolyzes the neurotransmitter acetylcholine (ACh) at cholinergic synapses by catalyzing the reaction. The great speed of the enzyme is essential for the rapid modulation of synaptic activity.[1,2] The crystal structure of *Tc*AChE[3] reveals that it combines a catalytic triad (His440-Glu327-Ser200) and a dipolar hole to catalyze substrate hydrolysis through an acylation−deacylation mechanism. As the first key step of the reaction, it reacts with ACh and produces a short-lived acetyl-enzyme (acylation).

Organophosphorus acid anhydrides (OPs) are rapid, stoichiometric, and essentially irreversible inhibitors of serine hydrolases. They can act as "hemisubstrate" to trap the enzyme.[4−8] Sarin (*O*-isopropylmethylphosponofluoridate) is one of the well characterized OP inhibitors. When sarin interacts with AChE, it blocks the active center of AChE by the phosphonylation on Ser200. The phosphonylation yields a considerably more stable sarin−serine adduct and is more stereospecific than acylation. This results in the inhibition of the enzyme action. The sarin−AChE adduct has been proposed to undergo dealkylation by a carbonium ion mechanism, resulting in C−O bond breaking and total loss of enzyme activity of AChE.

Biological activity of molecules crucially depends on the electronic structure of the active part of the given compound and its conformation. Different chemical structures either permit or forbid the biological catalytic reaction to take place for purely sterical reasons. The previous studies have demonstrated that both the conformation and the electronic structure of the various sarin conformers may play important roles in the preliminary steps of the sarin-related chemical reactions.[9−11] However, the structure of sarin−serine adduct becomes more complex than sarin itself due to the orientation of the functional groups (Figure 1).

The results of recent theoretical studies suggest that the treatment of the entire triad and some additional residues might be crucial for the inhibition of acetylcholinesterase.[12−16] However, sarin forms a considerably more stable product with Ser200 through the phosphonylation process than the acylation product with ACh as the enzyme is supposed to react.[4,9] The differences in chemical structures of these sarin−serine conformers could significantly influence either the biological catalytic activity of the enzyme or the alkylation and the dealkylation reaction processes at the early stage and thus would lead to the inhibition of the enzyme action. Therefore, the theoretical study of similarities and differences in the electronic structure and geometry of sarin−serine compound is worth undertaking. This may lead to better understanding the basis for irreversible inhibition of nerve agent on serine and the dealkylation process of the adduct and might help to detect, decontaminate, and destruct this deadly compound.

Since there is a number of possible diverse structures of the sarin−serine adduct, an effective method needs to be employed to search the local energy minima and the global minimum. Generally, the thermodynamically most stable structure should be located by the efficient structure prediction; that is, the structure with the lowest free energy should be identified. Since this is computationally impractical, a common simplification is to search the global minimum of the potential energy surface. The main obstacles in locating the most stable (global-minimum) structure are the existence of numerous local minima and the high dimensionality of the potential energy surface. Other

* To whom correspondence should be addressed.
[†] Jackson State University.
[‡] Wroclaw University of Technology.
[§] Shanghai Institutes for Biological Sciences.

10.1021/jp040574g CCC: $30.25
Published on Web 12/14/2004

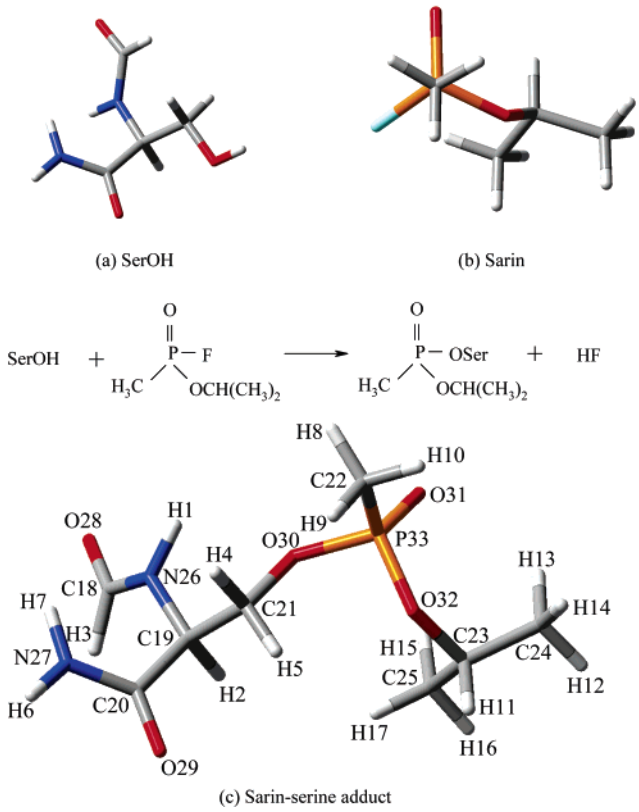

Figure 1. Structures of serine, sarin and sarin−serine adduct.

difficulties include the large number of interatomic interactions that must be considered in the energy computations of adduct species.[17]

The location of the global minimum by an exhaustive search of configuration space takes a large amount of time, even for moderate size systems. Widely used unbiased global minimization algorithms include various versions of simulated annealing, genetic algorithms, multicanonical methods, classical density annealing methods, and quantum annealing methods.[18]

Due to the importance of the knowledge of sarin's properties for development of efficient technologies of its deactivation and destruction, we have recently performed investigations of its conformers and stabilities,[9] adsorption and decomposition on soil[10] and MgO.[11] In this study, the DFT-based molecular dynamics approaches are applied to obtain the structural fluctuation trajectories of the sarin−serine adducts. The quantum chemistry calculations are then used to explore the energy properties of the local energy minimum structures predicted in the MD trajectory search. For the studied conformers, the Gibbs free energy and the Boltzman probability distribution law have been applied to three different temperatures in order to verify the global minimum structure in the sarin−serine adduct simulated space.

2. Computational Methods

The principles of ab initio molecular dynamics method are described in refs 19−23. The Vienna Ab Initio Simulation Package (VASP) program[24−27] was used to obtain the trajectory of various conformers of sarin−serine adduct.

The sarin−serine adduct was located in a cubic box with a length of 13 Å. A plane-wave basis set with the cutoff energy of 396 eV has been used for the electron wave function which was solved at each MD step by conjugate gradient minimization of the total electronic energy. One single k-point is applied for the simulation. The Perdew-Wang[28] gradient correction has been added to the exchange-correlation functional.[29] For the core region, the optimized Vanderbilt ultrasoft pseudopotentials[30] supplied with the VASP package[31,32] have been used for C, N, O, P, and H atoms.

The time-step applied was 0.5 fs, and the length of the simulation was 4.0 ps. The corresponding simulation temperature was set to 1000 K. The MD simulations were performed using the Nosé-Hoover thermostat[33,34] for the temperature control. All the ions positions have been recorded in each step. There are 8000 configurations of the adduct recorded through the equilibrium simulation. For every 200 steps, one configuration has been selected from the equilibrium trajectory. Forty configurations have been chosen evenly as the initial structures from the trajectory for the study of adduct conformations.

To illustrate how the temperature influences the conformation and to avoid missing conformations which may need to overcome higher energy barriers, a simulation trajectory was also carried out at 2000 K simulated temperature. This high temperature was used in the simulations to generate efficiently the possible conformations.

The local energy minimum structures predicted in the MD trajectory study have been fully optimized by the analytic gradient techniques using the density functional theory with the Becke's three parameter (B3)[35] exchange functional along with the Lee−Yang−Parr (LYP) nonlocal-correlation functional[36,37] (B3LYP). The standard valence triple-ζ basis set augmented with d-type and p-type polarization functions, 6-311G(d,p),[38] was used for C, N, O, P, and H atoms. The frequency analysis was also performed at the B3LYP/6-311G(d,p) level of theory to identify the local minimum energy structures. For the verification of the accuracy of the B3LYP/6-311G(d,p) level relative energies of the sarin−serine adduct, the second order of the Møller−Plesset perturbation theory (MP2)[39−41] was applied to perform the single-point calculations at the B3LYP/6-311G(d,p) optimized geometries. The Gaussian 98 program package[42] was used for this part of the study.

3. Results and Discussions

Through the optimization of 40 initial structures selected evenly from the MD trajectory, 20 different conformers have been located as the local minima on the potential energy surface of sarin−serine adduct at the B3LYP/6-311G(d,p) level of theory. Since the spatial location of the isopropyl group attached to O32 of sarin moiety influences the phosphonylation and the dealkylation process (the enzyme "aging" procedure), it is natural to classify the sarin−serine adduct according to the relative orientations of the isopropyl group. The optimized structures located in our study have been categorized into five classes according to the arrangements of the isopropyl group (depicted in Figure 2). In Class 1, two methyl groups of the isopropyl group lie almost in the plane of O31−P33−C23. Class 2 is related to Class 1 by rotating the isopropyl group around the O32−C23 bond by about 140°. Further rotation of the isopropoxyl group in Class 2 around the P33−O32 bond by approximate 50° leads to Class 3. The rotation of the isopropyl group in Class 3 around the O32−C23 bond by additional angles of 175° and 220° yields Classes 4 and 5, respectively.

For these five classes of the sarin−serine adduct, Class 1 includes five different conformers, Class 2 contains three, Class 3 consists of seven, Class 4 comprises four, and Class 5 has one conformer, respectively. Among all of the 40 initial structures being optimized, thirteen fall into Class 1, four into

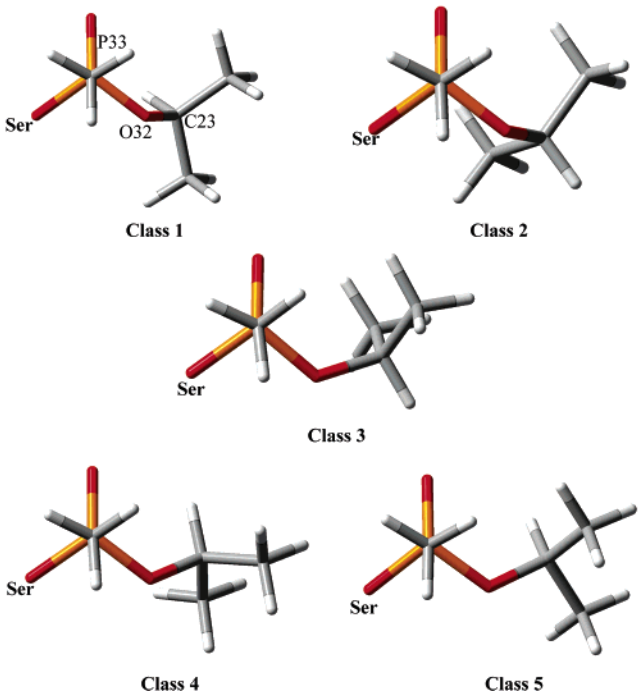

Figure 2. Five classes of sarin−serine adduct according to the arrangement of the isopropyl group (see text for the definition).

Class 2, eleven into Class 3, nine into Class 4, and three into Class 5. The energies and the lowest vibrational frequencies of each conformer are listed in Table 1.

3.1. Geometries and the Stability of Sarin−Serine Adduct Conformers. *Class 1 (Figure 3).* The most stable conformer in Class 1 is **1**−**1**. It has also the lowest energy among all the twenty conformers (−1142.16068 au after the zero-point energy correction). From the forty evenly selected initial structures, six lead to **1**−**1** through the optimization procedure. The intramolecular H-bond between H7 and O31 of the phosphinyl is revealed with the atomic distance of 1.96 Å. This strong H-bonding interaction is expected to stabilize **1**−**1**. The serine moiety of **1**−**1** extends to the opposite direction of the sarin, indicating that the influence of the serine moiety on the orientation of the isopropyl group is negligible in this conformer. The lowest vibrational frequency is amounted to 19 cm^{-1} and the vibrational mode corresponds to the rotation of the isopropyl group around the O32−C23 bond.

1−**2** is the second most stable adduct in Class 1, about 2.7 kcal mol^{-1} higher in energy than **1**−**1**. Four out of the 40 initial structures result in **1**−**2** conformations. A H-bond between H7 and O30 (which is the bridging site of serine and sarin moieties) is formed with the bond length of 2.05 Å. The rotation of the isopropyl group is partly blocked by the spatial effects of the serine part. Consequently, the lowest vibrational frequency exhibits the rotation motion of both serine and sarin moieties around C21−O30 bond.

Optimizations of two out of the 40 initial structures lead to **1**−**3**. The arrangement of the serine moiety in **1**−**3** is similar to that of **1**−**2**, and the only difference lies in the dihedral angle of P33−O30−C21−C19. It amounts to 109.3° and 93.9° for **1**−**2** and **1**−**3**, respectively. The energy difference between **1**−**2** and **1**−**3** is negligible (only 0.7 kcal mol^{-1}), suggesting that the stabilities of **1**−**2** and **1**−**3** are virtually the same. The atomic distance of H7 and O30 has been evaluated to be 2.07 Å, indicating a moderate strength of H-bond. Similar to **1**−**2**, the rotation of the isopropyl group in **1**−**3** is hindered by the spatial influence of serine moiety. The lowest vibrational frequency of **1**−**3** corresponds to the collaborative rotation of the serine and sarin moieties around the O30−P33 bond. The small value of this lowest vibrational frequency implies a very flat potential energy surface of **1**−**3**.

The energy of **1**−**4** is 5.5 kcal mol^{-1} higher than that of **1**−**1**. No intramolecular H-bond is detected in **1**−**4**. Similar to **1**−**1**, the serine moiety spreads out to the opposite direction of sarin fragment and is expected to have little influence on the orientation of the isopropyl group. The first vibrational frequency corresponds to the rotation of the isopropyl group around the O32−C23 bond, which resembles the first vibrational mode in **1**−**1**.

1−**5** has the highest energy in Class 1. The energy difference between **1**−**5** and the most stable **1**−**1** is predicted to be 6.5 kcal mol^{-1}. No H-bond is observed in **1**−**5**. Similar to **1**−**2**, the spatial orientations of serine moiety restrain to some extent the rotation of the isopropyl group in sarin moiety. The lowest vibrational frequency of **1**−**5** is calculated to be 19 cm^{-1}, corresponding to the vibrational motion of the C19−C21−O30−P33 dihedral angle.

Two main factors seem to influence the stability of the conformers in Class 1. The formation of the intramolecular H-bond stabilizes the conformers. Among the five conformers of Class 1, H-bonds have been found only in **1**−**1**, **1**−**2**, and **1**−**3**. These three conformers are more stable than the other two (**1**−**4** and **1**−**5**) with no H-bonds. The other stabilizing factor is the relative spatial orientation of the serine moiety. Without the spatial obstruction of serine moiety **1**−**1** is more stable than **1**−**2** and **1**−**3,** whereas **1**−**4** appears to be more stable than **1**−**5**. This suggests that the spatial interaction between serine moiety and sarin fragment destabilizes the conformers. However, the spatial influence is less important than the H-bonding interaction. This can be seen from the fact that **1**−**2** and **1**−**3** are 2.5 ∼ 2.9 kcal mol^{-1} more stable than **1**−**4**.

Class 2 (Figure 4). Class 2 can be obtained through the rotation of the isopropyl group in Class 1 around the O32−C23 bond. Three conformers are classified as members of this class.

2−**1** is the most stable conformer in Class 2. However, it is 6.2 kcal mol^{-1} higher in energy than **1**−**1**. In **2**−**1**, the serine moiety stretches out to the opposite direction of sarin fragment. There is hardly any mutual spatial influence between the sarin and the serine moieties so that there is no restriction for the rotation of these two fragments. This can be seen from the first vibrational mode at 23 cm^{-1}, which corresponds to the collaborative rotation of serine and sarin moieties around the O30−P33 bond.

Two out of the 40 initial structures conveyed to **2**−**2**. The serine moiety of **2**−**2** is located at the vertical direction of the sarin fragment. The carboxyl terminal and the amino terminal of serine moiety point to the opposite direction of sarin part. The spatial influence in **2**−**2** seems to be moderate. It can be justified by its energy which is 2.0 kcal mol^{-1} higher than that of **2**−**1**.

The energy of **2**−**3** has been calculated to be 4.0 kcal mol^{-1} higher than that of **2**−**2**. The serine moiety in **2**−**3** has the similar vertical arrangement as that in **2**−**2**. However, the amino terminal of serine moiety in **2**−**3** is oriented toward the sarin direction. The 4.0 kcal mol^{-1} of extra energy in **2**−**3** suggests that the spatial influence of serine moiety for **2**−**3** is more important than for **2**−**2**. The first corresponding vibrational mode agrees with that of **2**−**1**.

No H-bond is formed in any of the three conformers in Class 2. It is clear that the spatial orientation and the interactions

TABLE 1: Energy Differences (B3LYP amd MP2) and the Lowest Vibrational Frequencies (B3LYP) of Studied Conformers[a]

classes	conformers	ΔE (kcal/mol) B3LYP	ΔE^s (kcal/mol) MP2[b]	ΔE^0_{ZP}[c] (kcal/mol) B3LYP	lowest vibrational frequency(cm^{-1})
1	**1−1**	0(−1142.42826)	0(−1139.74171)	0(−1142.16068)	19
	1−2	2.9	2.9	2.7	19
	1−3	3.1	2.7	3.0	7
	1−4	6.0	6.0	5.5	18
	1−5	7.1	6.3	6.5	19
2	**2−1**	6.3	6.4	6.2	23
	2−2	8.4	7.8	8.2	15
	2−3	13.0	12.2	12.2	21
3	**3−1**	3.1	3.8	3.1	11
	3−2	3.7	2.7	3.9	17
	3−3	4.0	3.4	4.1	19
	3−4	4.6	4.9	4.4	14
	3−5	4.9	3.5	5.1	27
	3−6	5.0	4.1	5.0	16
	3−7	5.4	5.6	5.2	9
4	**4−1**	1.2	2.5	1.1	16
	4−2	2.0	1.9	2.0	22
	4−3	3.5	3.9	3.1	21
	4−4	7.0	6.6	6.6	8
5	**5−1**	2.1	1.0	2.1	21

[a] Values Given in parentheses are the conformer **1−1** reference energies (in Hartree). [b] Single-point MP2 calculations for the B3LYP/6-311G(d,p) optimized geometries. [c] Zero-point corrected energy differences at B3LYP/6-311G(d,p) level.

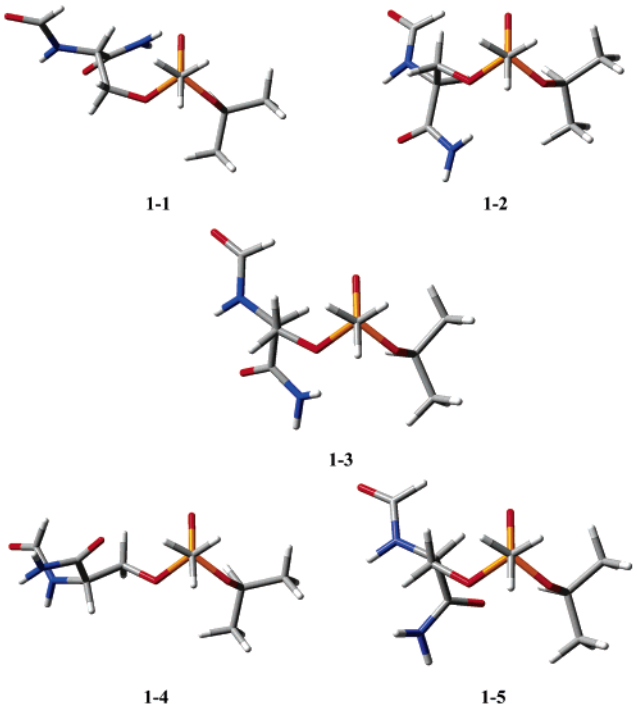

Figure 3. Sarin−serine conformers of Class 1.

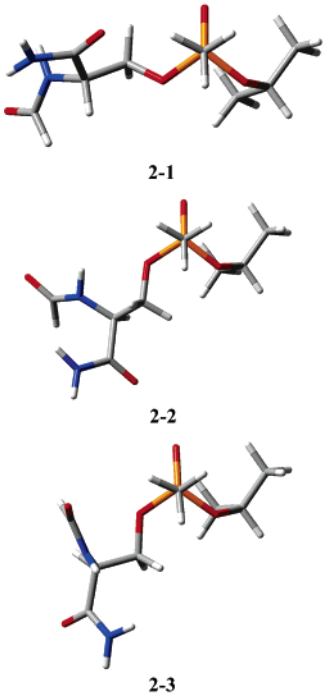

Figure 4. Sarin−serine conformers of Class 2 (obtained from Class 1 through rotation of the isopropyl group around the O32−C23 bond by 140°).

between the serine moiety and the sarin moiety dominate the relative stability of the conformers in this class.

Class 3 (Figure 5). Class 3 can be obtained by the rotation of the isopropoxyl group of Class 2 around the P33−O32 bond. It contains seven different conformers.

The lowest energy conformer in Class 3 is **3−1**, which is evaluated to be 3.1 kcal mol^{-1} higher than **1−1**. The atomic distance between H7 and O31 of the phosphinyl is estimated to be 1.9 Å, suggesting a strong H-bond which is expected to stabilize the conformer. The serine moiety is located at the opposite direction of sarin fragment which suggests that there is no spatial obstruction in **3−1**.The first vibrational mode of **3−1** is predicted at 11 cm^{-1}, corresponding to the rotation of the isopropoxyl group around the O32−P33 bond.

Optimization of four of the forty initial structures leads to **3−2**. It is only by ∼0.8 kcal mol^{-1} higher than **3−1**. A H-bond predicted between H7 and O32 is characterized by the distance of 2.07 Å. The serine moiety points to the vertical direction of the sarin moiety, indicating that spatial interactions between the two moieties exists in this conformer. The first vibrational mode corresponds to the collaborative rotation of the sarin and serine moieties around the P33−O30 bond.

Unlike **3−2**, no H-bond is predicted for **3−3**. However, the serine moiety extends toward the opposite direction of sarin fragment and has no spatial influence. The relative stabilities of **3−2** and **3−3** are so close that their energy difference is only about 0.2 kcal mol^{-1}. It implies that the spatial interaction

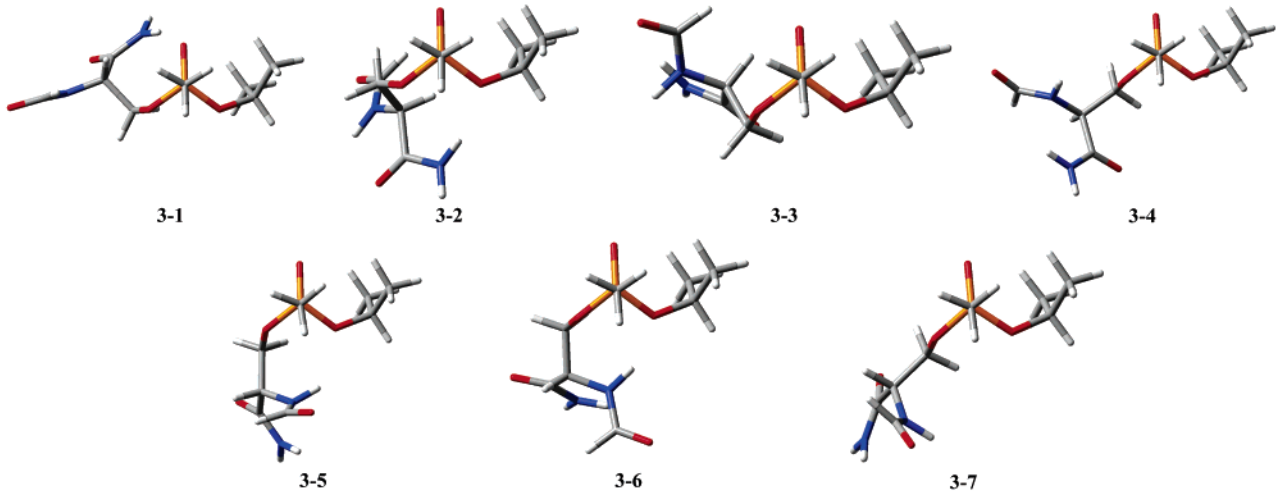

Figure 5. Sarin−serine conformers of Class 3 (obtained from Class 2 through rotation of the isopropoxyl group around the P33−O32 bond by 50°).

which destabilizes the adduct in **3**−**3** is balanced by the H-bonding interaction in this species. The character of the first vibrational mode of **3**−**3** is similar to that of **3**−**2**.

The difference of the orientation of serine moiety between **3**−**4** and **3**−**3** manifests itself the different arrangement of the carboxyl terminal and the amino terminal. However, this difference causes only insignificant energy difference between these two conformers (0.3 kcal mol^{-1}).

The energy of **3**−**5** is estimated to be 2.1 kcal mol^{-1} higher than **3**−**1**. The atomic distance between H1 and O32 is evaluated to be 2.25 Å, implying a weak H-bonding interaction that stabilizes **3**−**5**. However, the serine moiety is located at the vertical direction of the sarin moiety, destabilizing the adduct through spatial influence on the sarin moiety. The lowest vibrational frequency of **3**−**5** is calculated to be 27 cm^{-1}, corresponding to the cooperative rotation of the two moieties around the C21−C19 bond.

A H-bond between H1 and O32 with the bond length of 2.06 Å that stabilizes this conformer is revealed in **3**−**6**. Similar to **3**−**2**, the serine moiety of **3**−**6** is also oriented toward the vertical direction of the sarin fragment. However, the arrangement for the carboxyl and the amino terminal groups in serine moiety appears to be different in **3**−**2** and **3**−**6**. This structure difference results in slight energy difference (1.1 kcal mol^{-1}). The first vibrational mode is the same as that in **3**−**2**.

Two initial structures yielded the **3**−**7** through optimization process. The energy difference between **3**−**7** and **3**−**1** is calculated to be less than 2.2 kcal mol^{-1}. The molecular structure of **3**−**7** is similar to that of **3**−**4.** However, the orientation of the carboxyl and the amino terminal groups in serine moiety appears to be different for these two conformers. The first vibrational frequency of **3**−**7** is predicted at 9 cm^{-1}, corresponding to the cooperative rotation of the two fragments around the C21−O30 bond. The small value of this lowest frequency also suggests a flat potential energy surface around **3**−**7**.

As shown in Figure 5, **3**−**1** is the most stable conformer in Class 3. It is stabilized by both the intramolecular H-bond and the absence of spatial obstruction.

For the **3**−**3**, **3**−**4**, and **3**−**7** conformers, the serine moiety stretches out to the opposite direction of the serin moiety and there is no spatial influence of serine fragment on sarin part. The energy difference among these three conformers is less than 1.1 kcal mol^{-1}, which is mainly due to the different spatial direction of the carboxyl and the amino terminal groups of the serine moiety.

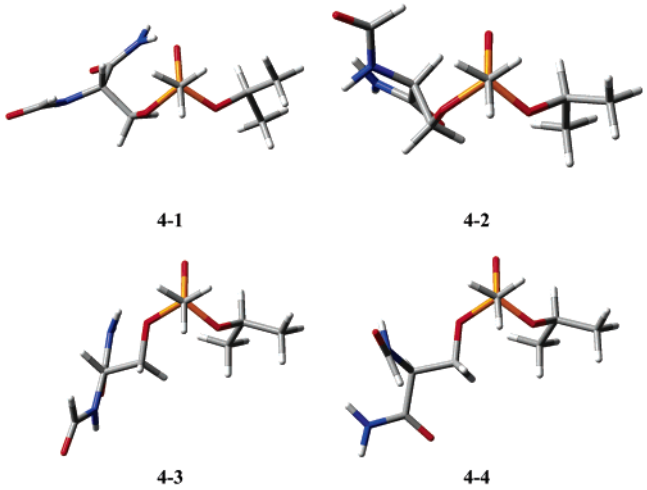

Figure 6. Sarin−serine conformers of Class 4 (obtained from Class 3 through rotation of the isopropyl group around the O32−C23 bond by 175°).

On the other hand, in all **3**−**2**, **3**−**5**, and **3**−**6** conformers, the serine moiety has spatial influences on the sarin part which destabilizes the related conformers. Meanwhile, H-bond is revealed in these three conformers and it stabilizes the corresponding conformers. The spatial repulsion is compensated by the H-bonding interaction.

For **3**−**2** to **3**−**7**, energy differences among the conformers amount to a relatively small value. The largest energy difference (between **3**−**2** and **3**−**7**) is less than 1.3 kcal mol^{-1}. In consequence, the stabilities of these six conformers in Class 3 are virtually the same.

Class 4 (Figure 6). Class 4 can be derived from the rotation of isopropyl group in Class 3 around the O32−C23 bond for about 175 °. There are four conformers in this class.

4−**1** is the most stable structure in Class 4. Three from the 40 initial structures result in **4**−**1**. It is about 1.14 kcal mol^{-1} higher in energy than **1**−**1**. It has the same orientation of serine moiety as that of **3**−**1**, implying that **4**−**1** can be obtained directly from **3**−**1** through the rotation of isopropyl group around O32−C23 bond. **4**−**1** has been evaluated to be 1.9 kcal mol^{-1} more stable than **3**−**1**. A H-bond which stabilizes **4**−**1**

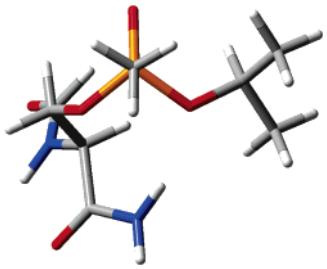

5-1

Figure 7. Sarin−serine conformers of Class 5 (obtained from Class 3 through rotation the isopropyl group around the O32−C23 bond by 220°).

has been predicted between H7 and O31 of phosphinyl with the distance of 1.92 Å. The first vibrational mode of **4**−**1** is predicted at 16 cm^{-1}, corresponding to the rotation of the serine and sarin moieties around the O30−P33 bond.

Two from the 40 initial structures are optimized to **4**−**2**. The arrangement of serine moiety in **4**−**2** is the same as that of **3**−**2**, suggesting that **4**−**2** can be directly derived from **3**−**2** by rotating the isopropyl group around the O32−C23 bond. However, **4**−**2** has been calculated to be 2.1 kcal mol^{-1} lower in energy than **3**−**2**, suggesting that the orientation of sarin part of Class 4 might be more stable than that of Class 3. A small energy difference is observed between **4**−**2** and **4**−**1** (0.8 kcal mol^{-1}), implying their similar stabilities. The first vibrational mode of **4**−**2** corresponds to the rotation of isopropyl group around the O32−C23 bond.

There are three initial structures leading to **4**−**3**. It is about 2.0 kcal mol^{-1} higher in energy than **4**−**1**. A weak H-bond is revealed between H7 and O30 with the distance of 2.2 Å, which stabilizes **4**−**3** to some extent. Meanwhile, with the serine moiety locating at the vertical direction of sarin moiety, spatial influence destabilizes the species. The lowest vibrational frequency is predicted to be 21 cm^{-1}, mainly corresponding to the rotation mode of the isopropoxyl group around the O32−P33 bond.

4−**4** is estimated to be 5.4 kcal mol^{-1} higher in energy than **4**−**1**. No H-bond is observed. Spatial obstruction occurs in **4**−**4** as the serine moiety orients to the vertical direction of sarin moiety, which destabilizes the conformer. This spatial influence is supposed to hinder the rotation of the isopropyl group, confirmed by the first vibrational mode that shows the collaborative rotation of the serine and sarin moieties around the O30−C21 bond. The small value of the lowest frequency suggests a very flat potential energy surface around **4**−**3**.

Class 5 (Figure 7). There is only one conformer (**5**−**1**) in this class.

Among the 40 initial structures, three leaded to **5**−**1** through optimization procedure. It is predicted to be 2.1 kcal mol^{-1} higher in energy than **1**−**1**. A H-bond is revealed between H7 and O32 with the length of 2.09 Å. The serine moiety in **5**−**1** is arranged to the vertical direction of sarin part, which appears to be the same as that of **3**−**2**. Thus, **5**−**1** can be simply obtained by rotating the isopropyl group of **3**−**2** by 140° around the O32−C23 bond. **5**−**1** is evaluated to be 1.8 kcal mol^{-1} more stable than **3**−**1**, implying that under the same orientation of serine moiety, the structure of sarin moiety in Class 5 is preferable to Class 3. However, the fact that one conformer is obtained in Class 5 suggests that only with the similar stereo effects of serine moiety in **5**−**1** can Class 5 be stabilized. The lowest vibrational frequency of **5**−**1** is predicted at 21 cm^{-1}, corresponding to the rotation of the serine and sarin moieties around the O30−P33 bond.

Full geometry optimization of the initial structures obtained from the MD simulations revealed that among the twenty conformers, **1**−**1**, **2**−**1**, **3**−**1**, **4**−**1**, and **5**−**1** are the lowest energy structures in their own classes. From the 40 initial structures, thirteen are classified into Class 1, implying that Class 1 characterizes the most stable pattern for the adduct. The energy properties of the twenty sarin−serine conformers revealed in the present study suggest that at least four of the conformers (**1**−**1, 4**−**1, 4**−**2**, and **5**−**1**) are expected to have crucial contributions to the phosphonylation and dealkylation reactions of the sarin−serine adduct. Among them, the **1**−**1** conformer is the most important.

The single-point calculations at the MP2/6-311G(d,p) level were performed to verify the accuracy of the B3LYP/6-311G(d,p) approach. The results are shown in Table 1. The global minimum **1**−**1** conformer was also found to have the lowest energy in the MP2/6-311G(d,p) calculations. The energy differences between conformers studied at these two theoretical levels are smaller than 1.3 kcal/mol, indicating that the B3LYP/6-311G(d,p) approach is an economic and reliable choice for the present study.

Comparing the structures of the located sarin−serine conformers with the crystallographic data (PDB code: 1CFJ),[7] the **1**−**4** and **2**−**1** conformers are found to match the crystallographic arrangement. However, as discussed above, these two conformers are only about 5.9∼6.3 kcal/mol higher in energy than the lowest energy conformer **1**−**1**. The energy difference may be easily overcome by the interactions with the surrounding environments.

Three stable conformers were reported for the sarin molecule.[9] However, the sarin moiety as a part of the sarin−serine adduct in the present study can be classified into five classes. This observation suggests that some arrangements of the sarin structure, such as conformers in Class 5, can exist only under the influence of the serine presence.

3.2. Molecular Dynamics Results. In our DFT-based molecular dynamics study, equilibrium trajectories of the sarin−serine adduct were recorded up to 8000 time steps. The energy variation of the sarin−serine adduct under the simulation temperature of 1000 K is depicted in Figure 8. The energy fluctuation of 2.6 eV during the simulation indicates that the simulation is an equilibrating procedure. Different conformers of sarin−serine adduct are classified according to the relative orientations of the isopropyl group in the sarin moiety, which, in turn, can be characterized by the atomic distances of O31−C24, C22−C24, and C22−C25. The variation of these three characteristic atomic distances amounts to 2.2 Å for O31−C24, 2.3 Å for C22−C24, and 2.5 Å for C22−C25, respectively (Figure 9). During the data-collecting period of the MD simulation the highest peaks appeared around 1317 time step for O31−C24, 868 time step for C22−C24, and 2771 time step for C22−C25, respectively. On the other hand, the deepest gorges can be found around 4338, 1702, and 92 time steps for atomic distances of O31−C24, C22−C24, and C22−C25, respectively.

The increase of the simulating temperature raises the energy fluctuation, as can be seen in Figure 10, in which the largest energy variations observed are less than 6.4 eV during the equilibrium data-collecting process under the simulation temperature of 2000 K. However, the peculiarity that the highest peaks and deepest gorges of the three characteristic atomic distances appeared during the simulation can still be observed in the high temperature trajectory (Figure 11). The atomic distances vary within 2.6 Å for O31−C24, 2.8 Å for

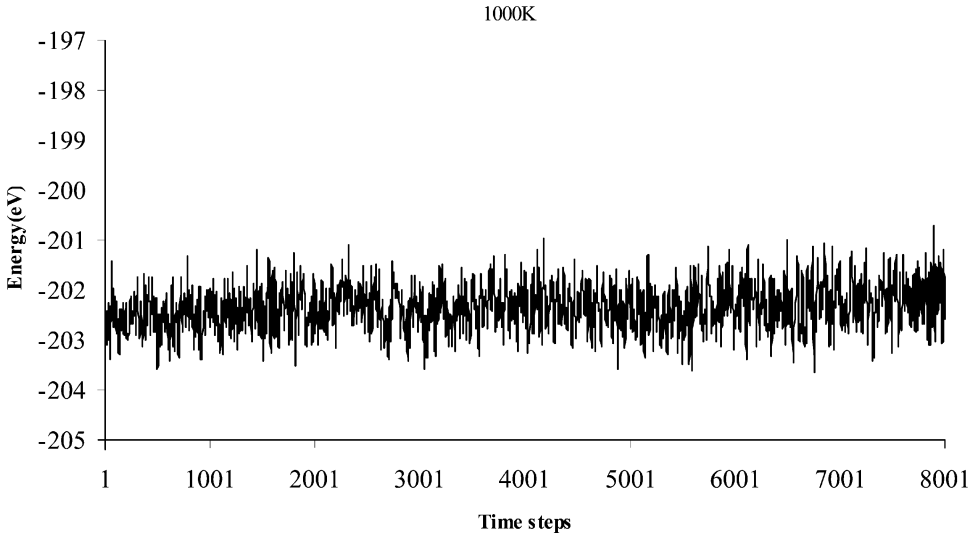

Figure 8. Energy fluctuation during 1000 K simulation process.

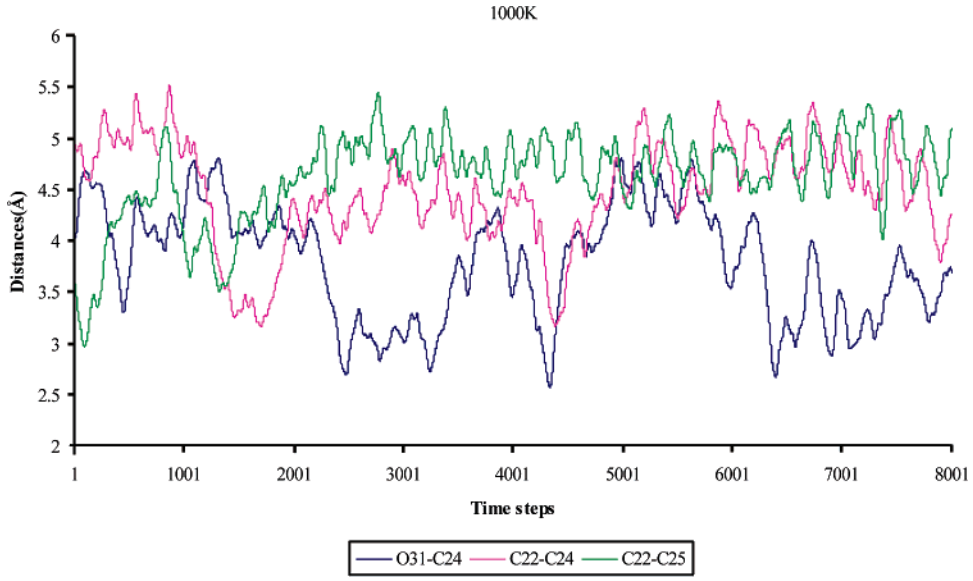

Figure 9. Characteristic atomic distance variation during 1000 K simulation.

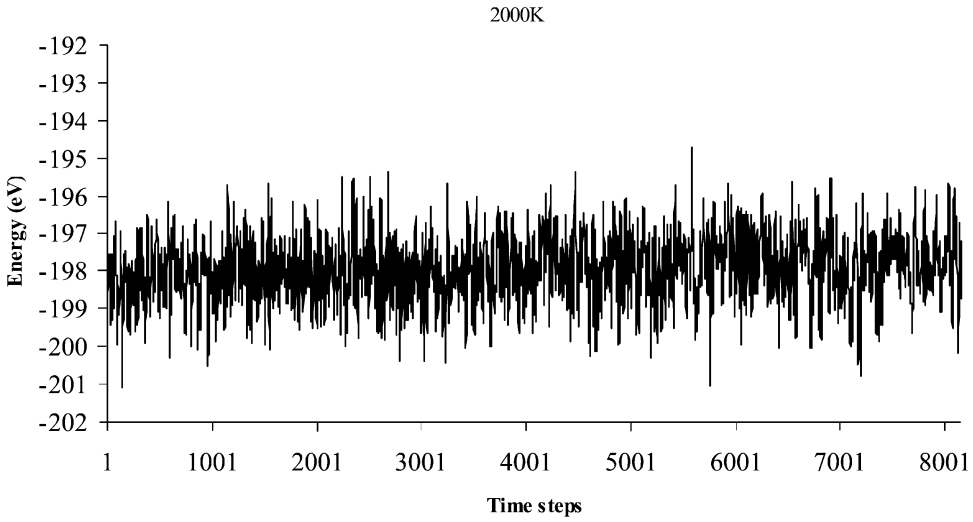

Figure 10. Energy fluctuation during 2000K simulation process.

C22−C24, and 2.9 Å for C22−C25, respectively. The similarity in geometric characteristics implies that the samples produced at these two different temperature simulations are similar.

The entropies and the Gibbs free energy differences of the twenty conformers at three different temperatures (298.15, 1000, and 2000 K, respectively) are shown in Table 2. Based on the

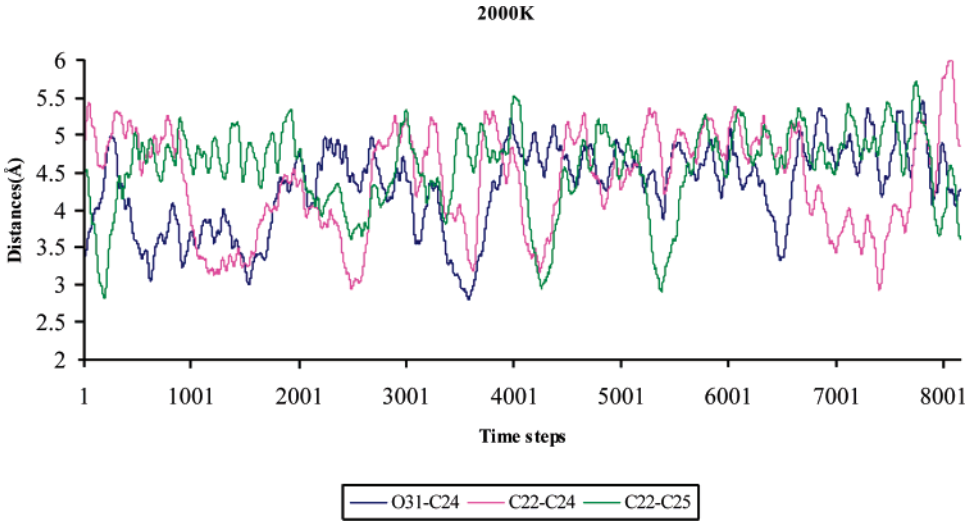

Figure 11. Characteristic atomic distance variation during 1000 K simulation.

TABLE 2: Entropies and the Gibbs Free Energy Differences of Studied Conformers under Three Different Temperatures

class	conformers	S(cal/mol)	$G^{298.15}$(a.u)	G^{1000}(a.u)	G^{2000}(a.u)
1	**1−1**	147.6	0(−1142.21063[a])	0(−1142.37575[a])	0(−1142.61102[a])
	1−2	150.0	2.1	0.4	−2.0
	1−3	150.6	2.2	0.1	−2.9
	1−4	149.9	5.1	3.5	1.2
	1−5	151.3	5.8	3.2	−0.5
2	**2−1**	146.1	6.7	7.7	9.3
	2−2	149.3	7.9	6.7	5.0
	2−3	152.1	11.3	8.1	3.6
3	**3−1**	149.0	2.6	1.7	0.4
	3−2	145.1	4.5	6.3	8.9
	3−3	146.8	4.3	4.9	5.7
	3−4	150.5	3.7	1.7	−1.2
	3−5	144.8	5.9	7.9	10.8
	3−6	146.6	5.3	6.0	7.0
	3−7	151.1	4.3	1.9	−1.6
4	**4−1**	149.3	0.7	−0.5	−2.2
	4−2	147.8	2.0	1.9	1.7
	4−3	149.1	2.8	1.8	0.2
	4−4	153.0	5.2	1.5	−3.9
5	**5−1**	145.8	2.7	4.0	5.9

[a] The values in parentheses correspond to the Gibbs free energy of conformer **1−1** in a.u. at the B3LYP/6-311G(d,p) level. The Gibbs free energy differences are based upon that of conformer **1−1**.

Gibbs free energy of the most stable conformer **1−1**, the Gibbs free energy differences of the other nineteen conformers vary as the temperature changes. When temperature increases, the Gibbs free energy differences decrease for conformers of **1−2**, **1−3**, **1−4**, **1−5**, **2−2**, **2−3**, **3−1**, **3−4**, **3−7**, **4−1**, **4−2**, **4−3**, and **4−4**, which indicate that the contribution of these conformers to the phosphonylation and dealkylation reactions of the sarin−serine adduct increases under relatively higher temperatures. On the other hand, the other six conformers (**2−1**, **3−2**, **3−3**, **3−5**, **3−6**, and **5−1**) are expected to have less influence upon the sarin−serine reactions when temperature becomes higher. It also can be seen that the conformers which have spatial obstructions have usually higher entropies than those without spatial influences. Therefore, those conformers characterized by larger entropy are expected to possess higher probability during the high temperature simulations.

The probability of the twenty conformers under different temperatures, which are calculated according to the Boltzmman probability distribution law, is listed in Table 3. The lowest energy conformer **1−1** has the largest relative probability of 0.69 and the next lowest energy conformer **4−1** has the relative probability of 0.23 under the room temperature (298.15 K). As the temperature rises, the distribution probabilities of those conformers with higher entropies increase too. The conformers **1−1**, **1−2**, **1−3**, and **4−1** are with the probability larger than

TABLE 3: Boltzman Distribution Probabilities of Conformers under Three Different Temperatures

class	conformers	298.15 K	1000 K	2000 K
1	**1−1**	0.69	0.14	0.06
	1−2	0.02	0.11	0.09
	1−3	0.02	0.13	0.12
	1−4	1.3×10^{-4}	0.02	0.04
	1−5	4.1×10^{-5}	0.03	0.06
2	**2−1**	9.1×10^{-6}	2.8×10^{-3}	0.01
	2−2	1.2×10^{-6}	4.8×10^{-3}	0.02
	2−3	3.5×10^{-9}	2.3×10^{-3}	0.02
3	**3−1**	0.01	0.06	0.05
	3−2	3.2×10^{-4}	0.01	0.01
	3−3	4.7×10^{-4}	0.01	0.01
	3−4	1.3×10^{-3}	0.06	0.08
	3−5	3.2×10^{-5}	2.5×10^{-3}	3.7×10^{-3}
	3−6	8.9×10^{-5}	0.01	0.01
	3−7	4.7×10^{-4}	0.05	0.08
4	**4−1**	0.23	0.17	0.10
	4−2	0.02	0.05	0.04
	4−3	0.01	0.06	0.05
	4−4	9.9×10^{-5}	0.06	0.15
5	**5−1**	0.01	0.02	0.01

0.1 at 1000 K. Under 2000 K, the notable increase of the distribution of those conformers with relative high energy can be noticed. Clearly, any conformers with lower energies should exist in the simulated trajectories with relatively larger distribution probabilities. Consequently, the lowest energy conformer **1**−**1** is the global minimum in the simulated space.

4. Conclusions

Based upon the results of combined ab initio molecular dynamics and quantum chemical approaches, 20 stable conformers of sarin−serine adduct were located as the local minima on the potential energy surface.

Different conformers have various contributions to the sarin−serine adductation reactions under different temperatures. The energy properties of the 20 sarin−serine conformers revealed in the present study suggest that at least four of the conformers (**1**−**1**, **4**−**1**, **4**−**2**, and **5**−**1**) are expected to have crucial contributions to the phosphonylation and dealkylation reactions of the sarin−serine adduct at low temperature. Among them, the **1**−**1** conformer which has both the lowest energy and the highest Boltzmann distribution relative probability is the most important. However, as temperature rises, the **4**−**1** conformer will play a more important role than **1**−**1** in the searin-serine reactions. Under the relatively high temperatures, the contribution of the **5**−**1** conformer decreases in the phosphonylation and dealkylation reactions while at least eight other conformers (**1**−**2**, **1**−**3**, **3**−**1**, **3**−**4**, **3**−**7**, **4**−**2**, **4**−**3**, and **4**−**4**) are expected to have stronger influences at the above-mentioned reactions.

Acknowledgment. This work was supported by the NSF CREST Grant HRD-0318519 and the Army High Performance Computing Research Center under the auspices of the Department of the Army, Army Research Laboratory cooperative agreement number DAAD19-01-2-0014 (modification12), the content of which does not necessarily reflect the position or the policy of the government, and no official endorsement should be inferred.

References and Notes

(1) Rosenberry, T. L. *Adv. Enzymol. Relat. Areas Mol. Biol.* **1975**, *43*, 103-218.
(2) Quinn, D. M. *Chem. Rev.* **1987**, *87*, 955−975.
(3) Sussman, J. L.; Harel, M.; Frolow, F.; Oefner, C.; Goldman, A.; Toker, L.; Silman, I. *Science* **1991**, *253*, 872−879.
(4) Taylor, P.; Lappi, S. *Biochemistry* **1975**, *14*, 1989−1997.
(5) Barak, D.; Ordentlich, A.; Kaplan, D.; Barak, R.; Mizrahi, D.; Kronman, C.; Segall, Y.; Velan, B.; Shafferman, A. *Biochemistry* **2000**, *39*, 1156−1161.
(6) Millard, C. B.; Koellner, G.; Ordentlich, A.; Shafferman, A.; Silman, I.; Sussman, J. L. *J. Am. Chem. Soc.* **1999**, *121*, 9883−9884.
(7) Millard, C. B.; Kryger, G.; Ordentlich, A.; Greenblatt, H. M.; Harel, M.; Raves, M. L.; Segall, Y.; Barak, D.; Shafferman, A.; Silman, I.; Sussman, J. L. *Biochemistry* **1999**, *38*, 7032−7039.
(8) Bencsura, A.; Enyedy, I. Y.; Kovach, I. M. *Biochemistry* **1995**, *34*, 8989.
(9) Kaczmarek, A.; Gorb, L.; Sadlej, A. J.; Leszczynski, J. *Struct. Chem.* **2004**, in press.
(10) Michalkova, A.; Gorb, L.; Ilchenko, M.; Zhikol, O. A.; Shishkin O. V.; Leszczynski, J. *J. Phys. Chem. B* **2004**, *108*, 1918−1930.
(11) Michalkova, A.; Gorb, L.; Leszczynski, J. *J. Phys. Chem. B* **2004**, *108*, 5294−5303.
(12) Saxena, A.; Viragh, C.; Frazier, D. S.; Kovach, I. M.; Maxwell, D. M.; Lockridge, O.; Doctor, B. P. *Biochemistry* **1998**, *37*, 15086−15096.
(13) Zhang, Y.; Kua, J.; McCammon, J. A. *J. Am. Chem. Soc.* **2002**, *124*, 10572−10577.
(14) Hurley, M. M.; Wright, J. B.; Lushington, G. H.; White, W. E. *Theor. Chem. Acc.* **2003**, *109*, 160−168.
(15) Raimondi, M.; Famulari, A.; Specchio, R.; Sironi, M.; Moroni, F.; Gianinetti, E. *J. Mol. Struct. (THEOCHEM)* **2001**, *573*, 25−42.
(16) Vasilyev, V. V. *J. Mol. Struct. (THEOCHEM)* **1994**, *304*, 129−141.
(17) Wawak, R. J.; Pillardy, J.; Liwo, A.; Gibson, K. D.; Scheraga, H. A. *J. Phys. Chem. A* **1998**, *102*, 2904−2918.
(18) Lee, Y. H.; Berne, B. J. *J. Phys. Chem. A* **2000**, *104*, 86−95.
(19) Car, R.; Parrinello, M. *Phys. Rev. Lett.* **1985**, *55*, 247.
(20) Parrinello, M. *Solid State Commun.* **1997**, *102*, 107.
(21) Remler, D. K.; Madden, P. S. *Mol. Phys.* **1990**, *70*, 921.
(22) Payne, M. C.; Teter, M. P.; Allan, D. C.; Arias, T. A.; Joannopoulos, J. D. *Rev. Mod. Phys.* **1992**, *64*, 1045.
(23) Tuckerman, M. E.; Ungar, P. J.; Vonrosenvinge, T.; Klein, M. L. *J. Phys. Chem.* **1996**, *100*, 12878.
(24) Kresse, G.; Fürthmuller, J. *Phys. Rev. B* **1996**, *54*, 11169.
(25) Kresse, G.; Hafner, J. *Phys. Rev. B* **1991**, *49*, 14251.
(26) Kresse, G.; Hafner, J. *Phys. Rev. B* **1993**, *47*, 558.
(27) Kresse, G.; Fürthmuller, J. *Comput. Mater. Sci.* **1996**, *6*, 15.
(28) Perdew, J. P. In *Electronic Structure of Solids* '*91*; Ziesche, P., Eschrig, H., Eds.; Academie Verlag: Berlin, 1991; p 11.
(29) Perdew, J. P.; Zunger, A. *Phys. Rev. B* **1981**, *23*, 5084.
(30) Vanderbilt, D. *Phys. Rev. B* **1990**, *41*, 7892.
(31) Kresse, G.; Hafner, J. *J. Phys.* **1994**, *6*, 8245.
(32) Kresse, G.; Hafner, J. *Phys. Rev. B* **1993**, *48*, 13115.
(33) Nosé, S. J. *Chem. Phys.* **1984**, *81*, 511.
(34) Hoover, W. G. *Phys. Rev. A* **1985**, *31*, 1695.
(35) Becke, A. D. *J. Chem. Phys.* **1993**, *98*, 5648.
(36) Lee, C.; Yang, W.; Parr, R. G. *Phys. Rev. B* **1988**, *37*, 785.
(37) Miehlich, B.; Savin, A.; Stoll, H.; Preuss, H. *Chem. Phys. Lett.* **1989**, *157*, 200.
(38) Hehre, W. J.; Radom, L.; Schleyer, P. R.; Pople, J. A. *Ab initio Molecular Orbital Theory*; Wiley: New York, 1986.
(39) Head-Gorden, M.; Pople, J. A.; Frisch, M. J. *Chem. Phys. Lett.* **1988**, *153*, 503.
(40) Frisch, M. J.; Head-Gordon, M.; Pople, J. A. *Chem. Phys. Lett.* **1990**, *166*, 275.
(41) Frisch, M. J.; Head-Gordon, M.; Pople, J. A. *Chem. Phys. Lett.* **1990**, *166*, 281.
(42) Frisch, M. J.; Trucks, G. W.; Schlegel, H. B.; Scuseria, G. E.; Robb, M. A.; Cheeseman, J. R.; Zakrzewski, V. G.; Montgomery, J. A., Jr.; Stratmann, R. E.; Burant, J. C.; Dapprich, S.; Millam, J. M.; Daniels, A. D.; Kudin, K. N.; Strain, M. C.; Farkas, O.; Tomasi, J.; Barone, V.; Cossi, M.; Cammi, R.; Mennucci, B.; Pomelli, C.; Adamo, C.; Clifford, S.; Ochterski, J.; Petersson, G. A.; Ayala, P. Y.; Cui, Q.; Morokuma, K.; Malick, D. K.; Rabuck, A. D.; Raghavachari, K.; Foresman, J. B.; Cioslowski, J.; Ortiz, J. V.; Stefanov, B. B.; Liu, G.; Liashenko, A.; Piskorz, P.; Komaromi, I.; Gomperts, R.; Martin, R. L.; Fox, D. J.; Keith, T.; Al-Laham, M. A.; Peng, C. Y.; Nanayakkara, A.; Gonzalez, C.; Challacombe, M.; Gill, P. M. W.; Johnson, B. G.; Chen, W.; Wong, M. W.; Andres, J. L.; Head-Gordon, M.; Replogle, E. S.; Pople, J. A. *Gaussian 98*, revision D.3; Gaussian, Inc.: Pittsburgh, PA, 1998.